# Investigation of Nanoantennas Using Surface Integral Equations and the Multilevel Fast Multipole Algorithm

**B. Karaosmanoğlu, U. M. Gür, and Ö. Ergül**
Department of Electrical and Electronics Engineering, Middle East Technical University, Ankara, Turkey

**Abstract**— A rigorous analysis of nanoantennas using surface integral equations and the multilevel fast multipole algorithm (MLFMA) is presented. Plasmonic properties of materials at optical frequencies are considered by using the Lorentz-Drude models and employing surface formulations for penetrable objects. The electric and magnetic current combined-field integral equation is preferred for fast and accurate solutions, which are further accelerated by an MLFMA implementation that is modified for plasmonic structures. The developed simulation environment is used to investigate popular bowtie structures with different material properties and to analyze interactions between pairs of nanoantennas.

## 1. INTRODUCTION

Nanoantennas, i.e., antennas designed for optical frequencies, have attracted the interest of many researchers [1–7]. Although the idea of using nanoscale antennas operating at visible lights, e.g., for harvesting solar energy, was purposed decades ago, realization of nanoantennas had to wait for the developments in nanotechnology. Recently, various nanoantennas have been designed, manufactured, and tested for diverse applications, including energy harvesting [3], optical sensing [4], and imaging. Along this direction, computational simulations of nanoantennas have become essential for designing and investigating these structures in alternative scenarios before their experimental realizations [8].

Computational analysis of nanoantennas using the conventional solvers may not be trivial. While nanoantennas are commonly made of highly conducting materials, such as silver and gold, scaled solvers with perfectly conducting assumptions fail to provide realistic and accurate modeling of nanoantennas. This is mostly due to different behaviors of metals at optical frequencies, namely plasmonic effects [9], which become dominating factors especially for nanoscale objects [10]. Incorporating plasmonic effects into the existing solvers is also a challenging task, especially for full-wave solvers. This challenge can partially be solved by resorting to Drude or Lorentz-Drude models that allow for macroscopic analysis via electromagnetic parameters. Specially, changing the electrical permittivity to a complex value with a negative real part based on these models leads to a direct analysis of a plasmonic structure using existing solvers developed for penetrable objects.

In this study, we investigate nanoantennas using surface integral equations and a powerful method, namely, the multilevel fast multipole algorithm (MLFMA). Among alternative formulations, we prefer the electric and magnetic current combined-field integral equation (JMCFIE) for accurate and fast iterative solutions using MLFMA [11]. JMCFIE is modified carefully by considering complex permittivity values with negative real parts. MLFMA is also updated for stability in handling complex wavenumbers with large imaginary parts, leading to rapidly decaying interactions. In this paper, after demonstrating the effectiveness of the developed solver on canonical problems, we present numerical simulations of bowtie nanoantennas at optical frequencies. Different material properties and frequencies are considered for single bowtie nanoantennas (see Figure 1). Electromagnetic interactions between pairs of nanoantennas and their effects in the power enhancement abilities are also investigated. Numerical results show that MLFMA is a strong alternative to space-discretization solvers for accurate and efficient full-wave analysis of nanoantennas.

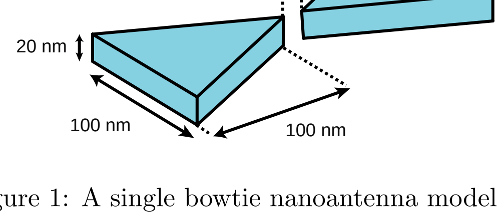


Figure 1: A single bowtie nanoantenna model [4].

## 2. MLFMA SOLUTIONS OF NANOANTENNAS

Consider a plasmonic object ($\epsilon_p$, $\mu_p$) located in a host medium ($\epsilon_o$, $\mu_o$) illuminated by incident electric and magnetic fields ($\mathbf{E}^{\mathrm{inc}}$, $\mathbf{H}^{\mathrm{inc}}$) created by external sources. Formulating the problem using JMCFIE discretized with the RWG functions, we obtain [12]

$$\begin{bmatrix} \bar{\mathbf{Z}}_{11} & \bar{\mathbf{Z}}_{12} \\ \bar{\mathbf{Z}}_{21} & \bar{\mathbf{Z}}_{22} \end{bmatrix} \cdot \begin{bmatrix} \mathbf{a}_J \\ \mathbf{a}_M \end{bmatrix} = \begin{bmatrix} \mathbf{w}_1 \\ \mathbf{w}_2 \end{bmatrix}, \tag{1}$$

where the matrix elements and the elements of the RHS vector are derived as

$$\bar{\mathbf{Z}}_{11} = \bar{\mathbf{Z}}_{22} = \bar{\mathbf{T}}_o^T + \bar{\mathbf{T}}_p^T + \bar{\mathbf{K}}_{PV,o}^N - \bar{\mathbf{K}}_{PV,p}^N - \bar{\mathbf{I}}^T \tag{2}$$

$$\bar{\mathbf{Z}}_{12} = -\eta_o^{-1}\bar{\mathbf{K}}_{PV,o}^T - \eta_p^{-1}\bar{\mathbf{K}}_{PV,p}^T - \frac{1}{2}\left(\eta_o^{-1} - \eta_p^{-1}\right)\bar{\mathbf{I}}^N + \eta_o^{-1}\bar{\mathbf{T}}_o^N - \eta_p^{-1}\bar{\mathbf{T}}_p^N \tag{3}$$

$$\bar{\mathbf{Z}}_{21} = \eta_o\bar{\mathbf{K}}_{PV,o}^T + \eta_p\bar{\mathbf{K}}_{PV,p}^T + \frac{1}{2}\left(\eta_o - \eta_p\right)\bar{\mathbf{I}}^N - \eta_o\bar{\mathbf{T}}_o^N + \eta_p\bar{\mathbf{T}}_p^N \tag{4}$$

$$\mathbf{w}_{1,2} = -\int_{S_m} d\mathbf{r}\mathbf{t}_m(\mathbf{r}) \cdot \left\{ \left[\eta_o^{-1}\mathbf{E}^{\mathrm{inc}}(\mathbf{r}) + \hat{\mathbf{n}} \times \mathbf{H}^{\mathrm{inc}}(\mathbf{r})\right], \left[\eta_o\mathbf{H}^{\mathrm{inc}}(\mathbf{r}) - \hat{\mathbf{n}} \times \mathbf{E}^{\mathrm{inc}}(\mathbf{r})\right] \right\}. \tag{5}$$

In the above, $\eta_u = \sqrt{\mu_u}/\sqrt{\epsilon_u}$ is the wave impedance for $u = \{o, p\}$. Discretized operators can be written as

$$\bar{\mathbf{T}}_u^{T,N}[m,n] = \int_{S_m} d\mathbf{r} \left\{\mathbf{t}_m(\mathbf{r}), \mathbf{t}_m(\mathbf{r}) \times \hat{\mathbf{n}}\right\} \cdot \mathcal{T}_u\{\mathbf{b}_n\}(\mathbf{r}) \tag{6}$$

$$\bar{\mathbf{K}}_{PV,u}^{T,N}[m,n] = \int_{S_m} d\mathbf{r} \left\{\mathbf{t}_m(\mathbf{r}), \mathbf{t}_m(\mathbf{r}) \times \hat{\mathbf{n}}\right\} \cdot \mathcal{K}_{PV,u}\{\mathbf{b}_n\}(\mathbf{r}) \tag{7}$$

$$\bar{\mathbf{I}}^{T,N}[m,n] = \int_{S_m} d\mathbf{r} \left\{\mathbf{t}_m(\mathbf{r}), \mathbf{t}_m(\mathbf{r}) \times \hat{\mathbf{n}}\right\} \cdot \mathbf{b}_n(\mathbf{r}), \tag{8}$$

where $\mathbf{t}_m$ and $\mathbf{b}_n$ represent testing and basis functions, respectively, and $\hat{\mathbf{n}}$ is the outward unit normal. Integro-differential operators are defined as

$$\mathcal{T}_u\{\mathbf{b}_n\}(\mathbf{r}) = ik_u \int d\mathbf{r}'\mathbf{b}_n(\mathbf{r}')g_u(\mathbf{r},\mathbf{r}') + \frac{i}{k_u}\int d\mathbf{r}'\nabla' \cdot \mathbf{b}_n(\mathbf{r}')\nabla g_u(\mathbf{r},\mathbf{r}') \tag{9}$$

$$\mathcal{K}_{PV,u}\{\mathbf{b}_n\}(\mathbf{r}) = \int_{PV} d\mathbf{r}'\mathbf{b}_n(\mathbf{r}') \times \nabla' g_u(\mathbf{r},\mathbf{r}'), \tag{10}$$

where $g_u(\mathbf{r},\mathbf{r}') = \exp(ik_u|\mathbf{r}-\mathbf{r}'|)/(4\pi|\mathbf{r}-\mathbf{r}'|)$, and $k_u = 2\pi/\lambda_u = \omega\sqrt{\mu_u}\sqrt{\epsilon_u}$ is the wavenumber for $u = \{o, p\}$. In MLFMA, the Green's function is factorized and diagonalized as

$$g_u(\mathbf{r},\mathbf{r}') = \frac{ik_u}{(4\pi)^2}\int d^2\hat{\mathbf{k}} \exp\left(ik_u\hat{\mathbf{k}} \cdot \mathbf{d}\right)\sum_{t=0}^{\mathcal{T}} i^t(2t+1)h_t^{(1)}\left(k_u D\right)P_t\left(\hat{\mathbf{k}} \cdot \hat{\mathbf{D}}\right), \tag{11}$$

where $\mathbf{r} - \mathbf{r}' = \mathbf{D} + \mathbf{d}$.

Consider a plasmonic object modeled with a permittivity of $\epsilon_p = -\epsilon_{pR} + i\epsilon_{pI}$. If $\epsilon_{pR} \gg \epsilon_{pI}$, then $\eta_p \approx -i\sqrt{\mu_p/\epsilon_{pR}}$, $k_p \approx i\omega\sqrt{\mu_p\epsilon_{pR}}$, and

$$\exp\left(ik_p\left|\mathbf{r}-\mathbf{r}'\right|\right) \approx \exp\left(-\omega\sqrt{\mu_p\epsilon_{pR}}\left|\mathbf{r}-\mathbf{r}'\right|\right) \tag{12}$$

is a rapidly decaying function. In other words, for highly plasmonic materials, inner interactions tend to be localized and captured by short-distance interactions. If the plasmonic object is located in a lossless and non-plasmonic medium, far-zone interactions in JMCFIE are dominated by the outer interactions. Then, depending on the target accuracy of matrix elements, contributions from the plasmonic material for some of the far-zone interactions can be omitted without deteriorating the accuracy of results. This approach leads to much faster matrix-vector multiplications, compared to using unnecessarily high numbers of harmonics required for large absolute values of wavenumbers encountered in highly plasmonic materials.

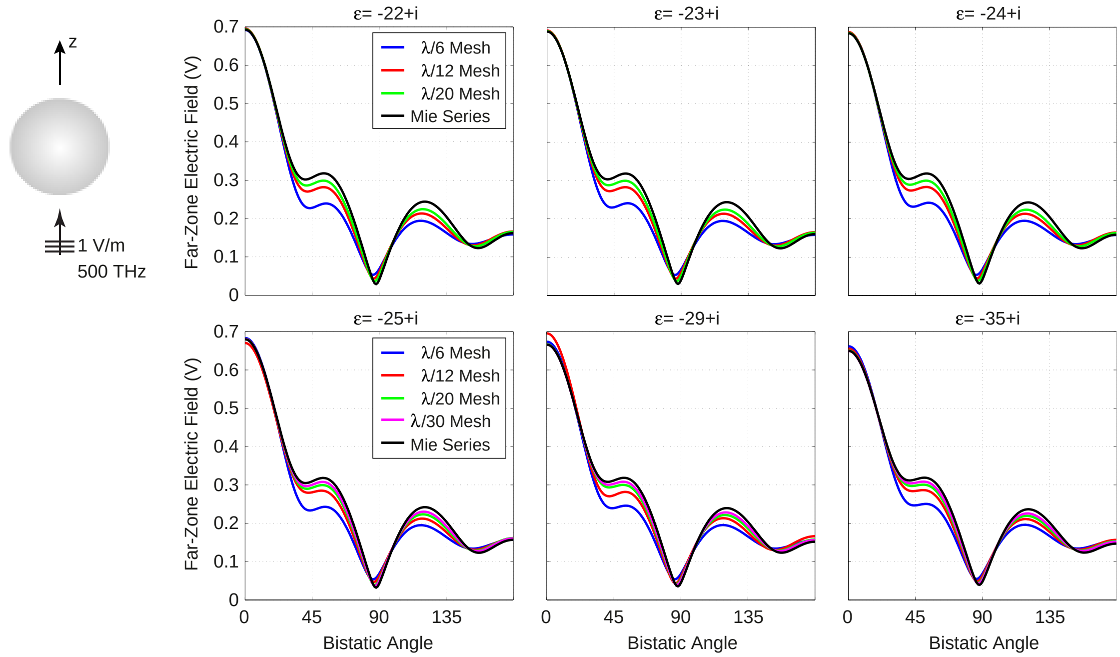


Figure 2: Solutions of scattering problems involving plasmonic spheres of radius 0.3 µm excited at 500 THz. MLFMA solutions obtained with different mesh sizes are compared to analytical Mie-series solutions.

## 3. NUMERICAL VERIFICATION

Figure 2 presents the results of numerical experiments involving spheres of radius 0.3 µm located in free space and illuminated by plane waves at 500 THz. Different relative permittivity values with unity imaginary parts and negative real parts from $-22$ to $-35$ are considered. Figure 2 depicts the far-zone electric field values on the $E$-plane with respect to the bistatic angle from 0 (forward-scattering direction) to 180° (backscattering direction). Computational values obtained by using the developed MLFMA implementation for different mesh sizes (i.e., $\lambda/6$, $\lambda/12$, $\lambda/20$, and $\lambda/30$, where $\lambda$ is the free-space wavelength) are compared to those obtained with analytical Mie-series solutions. For each case, it can be observed that the computational values converge to the reference Mie-series values as the mesh size is decreased and discretization is refined. In other words, the developed MLFMA solver provides controllable accuracy for plasmonic structures.

## 4. NUMERICAL RESULTS

Figure 1 depicts geometric details of the nanoantenna design considered in this study. The bowtie-shaped nanoantenna has two triangular prisms with 20 nm thickness and separated by 14 nm from tip to tip. The nanoantenna is investigated at optical frequencies when the Lorentz-Drude (LD) model is used to determine the complex permittivity of the materials. Figure 3 presents the results of numerical experiments involving single nanoantennas made of silver (Ag) and gold (Au), each illuminated by a plane wave (1 V/m) from 250 THz to 600 THz. The power density values in the vicinity of the nanoantennas are investigated with respect to the frequency. It can be observed that the nanoantennas become active in different ranges of frequencies, depending on the material. Specifically, power density values in the vicinity of the nanoantennas, especially at the feed locations between the tips, increase significantly at around 400 THz. High power density values indicate the focusing ability of the nanoantennas, hence suitability for energy harvesting.

For a quantitative comparison of different materials for the purpose of energy harvesting, Figure 4(a) presents the power enhancement ratio for single nanoantennas from 250 THz to 600 THz. In addition to silver (Ag) and gold (Au), copper (Cu) and platinum (Pt) materials are considered. Among these, platinum is known to show no plasmonic activity, therefore providing a baseline for the enhancement ability. The power density at the middle of the feed location is divided by the power density of the incident wave (plane wave) to calculate the power enhancement ratio with respect to the frequency. It can be observed that the enhancement ratio of the silver nanoantenna makes a peak at 410 THz with a value of 44.4. While the copper nanoantenna behaves similar to the silver nanoantenna in the 250–370 THz range, its peak occurs with a lower value at 390 THz, fol-

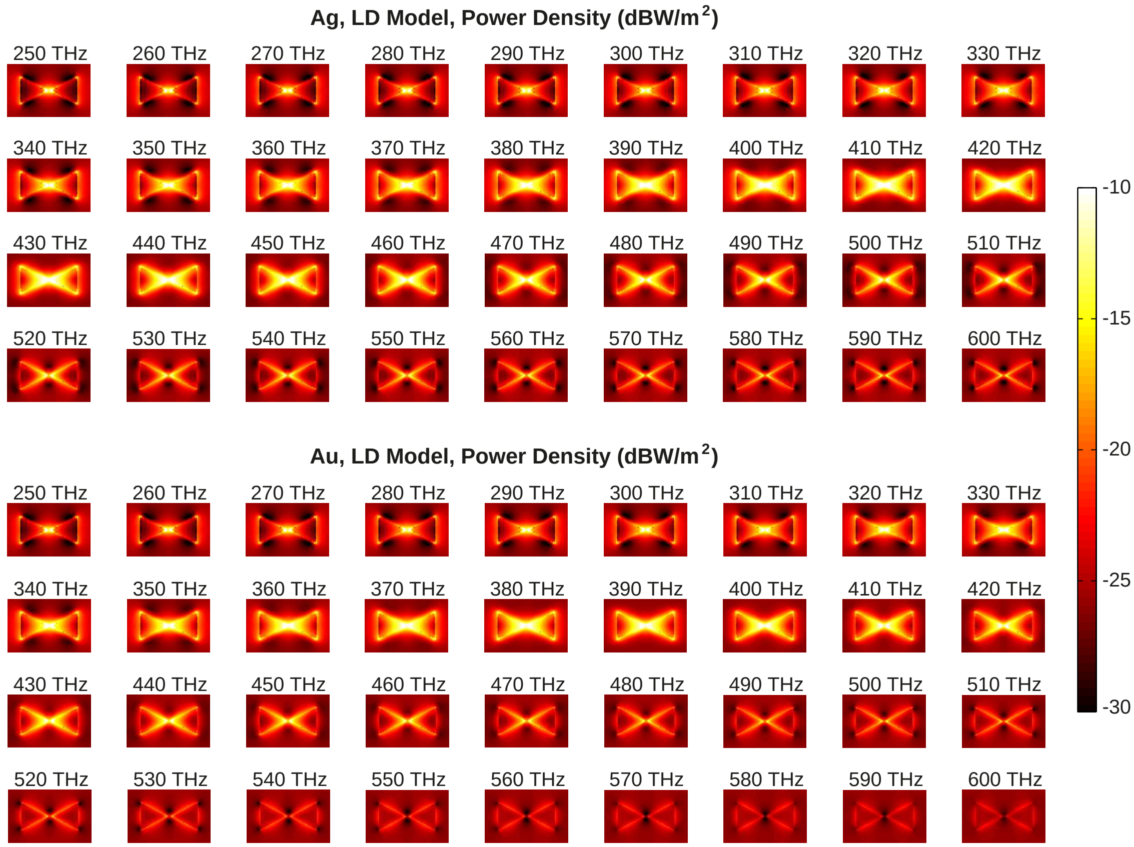


Figure 3: Power density values in the vicinity of single nanoantennas made of silver (Ag) and gold (Au), each illuminated by a plane wave (1 V/m) from 250 THz to 600 THz.

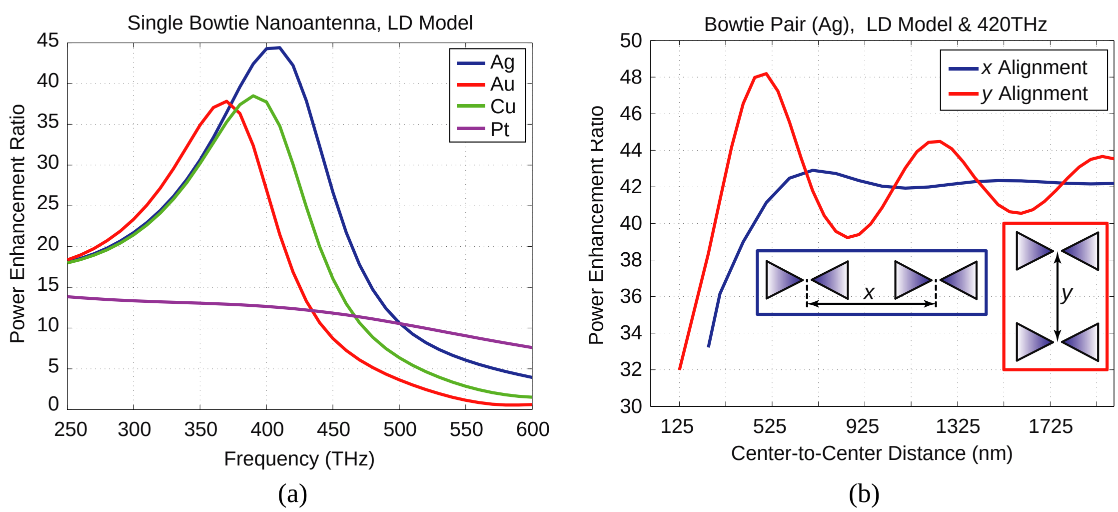


Figure 4: (a) The power enhancement ratio for single nanoantennas made of silver (Ag), gold (Au), copper (Cu), and platinum (Pt), each illuminated by a plane wave (1 V/m) from 250 THz to 600 THz. (b) The power enhancement ratio for a silver nanoantenna, while another identical nanoantenna approaches along $x$ and $y$ axis.

lowed by an earlier decay at higher frequencies. The peak and decay for the gold nanoantenna occur even earlier, and the enhancement ratio for this material is higher than the others from 250 THz to 370 THz, while the silver nanoantenna clearly outperforms the other nanoantennas after 390 THz. Finally, the enhancement ratio for the platinum decreases slowly from 13.8 to 7.6 in the entire range, providing a reference for measuring the performance of the plasmonic nanoantennas.

Finally, we consider pairs of silver nanoantennas and investigate the effect of mutual interactions on the enhancement ratios. Figure 4(b) presents the power enhancement ratio at the feed location of a nanoantenna, while another nanoantenna approaches along $x$ and $y$ axis. The frequency is fixed to 420 THz and the pairs are illuminated by plane waves. In both cases, the enhancement ratio tends to decrease when the nanoantennas become very close to each other. For some distances, however, higher ratios in contrast to the single-nanoantenna case are observed, especially for the $y$ alignment. Specifically, for the $y$ alignment scenario, an optimal distance from center to center is approximately 500 nm ($0.7\lambda$), leading to an enhancement ratio of 48.2. This information can be used to construct efficient nanoantenna arrays, while mutual couplings between array elements will be more complicated, needing further analysis with MLFMA.

## 5. CONCLUSION

Rigorous analysis of nanoantennas using surface integral equations and MLFMA is presented. The Lorentz-Drude model is used to formulate plasmonic effects at optical frequencies. Single nanoantennas with different materials, as well as pairs of nanoantennas in alternative scenarios are investigated. MLFMA provides accurate and efficient analysis of nanoantennas, while its potential will be revealed further for much larger nanoantenna systems.

## ACKNOWLEDGMENT

This work was supported by the Scientific and Technical Research Council of Turkey (TUBITAK) under the Research Grant 113E129 and by a BAGEP Grant from Bilim Akademisi — The Science Academy, Turkey.

## REFERENCES

1. Schuck, P. J., D. P. Fromm, A. Sundaramurthy, G. S. Kino, and W. E. Moerney, "Improving the mismatch between light and nanoscale objects with gold bowtie nanoantennas," *Phys. Rev. Lett.*, Vol. 94, 017402, 2005.
2. Alda, J., J. M. Rico-Garcia, J. M. Lopez-Alonso, and G. Boreman, "Optical antennas for nano-photonic applications," *Nanotechnology*, Vol. 16, 230–234, 2005.
3. Muhlschlegel, P., H.-J. Eisler, O. J. F. Martin, B. Hecht, and D. W. Pohl, "Resonant optical antennas," *Science*, Vol. 308, 1607–1609, 2005.
4. Kinkhabwala, A., Z. Yu, S. Fan, Y. Avlasevich, K. Mullen, and W. E. Moerney, "Large single-molecule fluorescence enhancements produced by a bowtie nanoantenna," *Nat. Photonics*, Vol. 3, 654–657, 2009.
5. Kosako, T., Y. Kadoya, and H. F. Hofmann, "Directional control of light by a nanooptical Yagi-Uda antenna," *Nat. Photonics*, Vol. 4, 312–315, 2010.
6. Krasnok, A. E., A. E. Miroshnichenko, P. A. Belov, and Y. S. Kivshar, "All-dielectric optical nanoantennas," *Opt. Express*, Vol. 20, No. 18, 20599–20604, 2012.
7. Chen, H., A. M. Bhuiya, L. Runyu, D. M. Wasserman, and K. C. Toussaint, Jr., "Design, fabrication, and characterization of near-IR gold bowtie nanoantenna arrays," *Phys. Chem. C*, Vol. 118, No. 35, 20553–20558, 2014.
8. Solis, D. M., J. M. Taboada, F. Obelleiro, and L. Landesa, "Optimization of an optical wireless nanolink using directive nanoantennas," *Opt. Exp.*, Vol. 21, No. 2, 2369–2377, 2013.
9. Johnson, P. B. and R. W. Christy, "Optical constants of the noble metals," *Phys. Rev. B*, Vol. 6, No. 12, 4370–4379, 1972.
10. Ergül, Ö., "Analysis of composite nanoparticles with surface integral equations and the multilevel fast multipole algorithm," *J. Opt.*, Vol. 14, No. 6, 062701-1–062701-4, 2012.
11. Ergül, Ö., "Solutions of large-scale electromagnetics problems involving dielectric objects with the parallel multilevel fast multipole algorithm," *J. Opt. Soc. Am. A*, Vol. 28, No. 11, 2261–2268, 2011.
12. Ergül, Ö. and L. Gürel, *The Multilevel Fast Multipole Algorithm (MLFMA) for Solving Large-scale Computational Electromagnetics Problems*, Wiley-IEEE, 2014.